Nigerian Research Journal of Engineering and Environmental Sciences 11(1) 2026 pp. 221-238
p ISSN: 2635-3342; e ISSN: 2635-3350

Nigerian Research Journal of Engineering and Environmental Sciences
Journal homepage: www.rjees.com

Original Research Article

Thermodynamic and Exergy-based Lifecycle Analysis of an Ejector Organic Rankine Cycle for Cooling and Power Generation

***Onwuzurike, I.G., Ntunde, D.I. and Ugwu, H.U.**

Department of Mechanical Engineering, Michael Okpara University of Agriculture, Umudike, P.M.B 7267, Umuahia, Abia State, Nigeria.
*ikechukwugreg06@gmail.com; ikechukwuonwuzurike@yahoo.com; ntunde.dilibe@mouau.edu.ng; ugwu.hyginus@mouau.edu.ng

http://doi.org/10.5281/zenodo.21047819

ARTICLE INFORMATION

Article history:
Received 29 Apr. 2026
Revised 29 May 2026
Accepted 29 May 2026
Available online 30 Jun. 2026

Keywords:
Energy
Exergy
Life cycle analysis
Organic Rankine cycle
Environmental impact

ABSTRACT

The study considered the investigation of a modified organic Rankine power-cooling cycle (ORPCC) integrated with an ejector system. The system comprises a vapour generator, turbine, an ejector, a pump, a throttling valve, an evaporator and a condenser and is driven by solar heat energy. Three organic refrigerants - R245fa, R1234yf and R1234ze were used for the analysis that covered exergy-based life cycle concept. The simulation of the system was done using a developed source code in Engineering Equations Solver (EES). The thermodynamic results show that the organic Rankine cycle (ORC) system configuration has a better energy and exergy efficiencies (up to 34.43, 28.87 and 32.38% energy efficiencies while 25.7, 31.27 and 31.68% exergy efficiencies for R245fa, R1234yf, and R1234ze, respectively). This enhancement was due to the additional cooling provided by the ejector refrigeration system (ERS), generating 151.9, 120.8, and 153 kW for R245fa, R1234yf, and R1234ze, respectively. The results further demonstrate that R1234ze and R245fa are thermodynamically better options for running the developed system. The system components using R245fa has the least environmental effect with a value of 518,830 mpts while the components using R1234yf has the highest environmental effect of 540,340 mpts. The environmental effect due to refrigerant leakage was highest when using R1234ze with a value of 933325.3 mpts while the least impact was 78,123.46 mpts for R1234yf respectively. The study recommends a multi-objective optimization of the plant in order to find the refrigerant that satisfies both the thermodynamic efficiency and environmental impact.

1. INTRODUCTION

The world today has largely achieved development through an increased efficient and extensive use of various forms of energy. Energy availability has become an important indicator for economic growth, industrialization and sustainable development (Gregory, 2025). The demand for energy has tended

towards our quest to sustain and improve our livelihood and with the progression in population growth, energy demand is expected to increase and widen (IEA Report*.,* 2025). Efforts to match this increasing population and economic development with adequate energy supply in many countries of the world have resulted in serious implications to the environment Ssali *et al.,* (2018). This is so because energy generation processes emit harmful pollutants which are injurious to the ecosystem (Ihim *et al*., 2023). These generation processes involving the burning of finite non-renewable energy source such as fossil fuel has contributed to the emission of large amount of greenhouse gases mostly carbon dioxide (Ukemeobong *et al.,* 2023).

The need for innovative energy conversion technologies has become so significant for sustainable power generation. In recent times, the vision is now towards assessing secured, environmentally friendly, renewable and sustainable primary energy resources. Solar energy heads these sources due to its availability and distribution in nature than other types of renewable energy sources. Solar energy resource which is a form of low grade heat source can be converted into electrical power, heating and cooling through the use of Organic Rankine Cycle, (ORC), providing a friendly, sustainable energy supply (Kolahi *et al.,* 2016). Its low cost of maintenance, simple in its application with low pressure requirements and high recovery efficiency makes it a very promising technology. The concept of the ORC system has become a welcomed technology that is characterized with high efficiency. Its principle is like those of the Rankine cycle but with organic fluid having high vapour pressure, lower boiling point than water, consisting of a pump, evaporator, turbine (which replaces the boiler) and a condenser. However, in addition to the foregoing and in an attempt to improve the ORC system efficiency, researchers have devoted their effort and attention towards reducing the pump work by modifying the basic ORC structure with other components such as an ejector to effect argumentation in turbine work, system efficiency and a reduction in the running cost of a combined power system. An ejector happens to be a passive compressor flow device that has no moving parts which is thermally activated by a high temperature/pressure fluid stream (primary fluid) and transferring the energy to a low pressure stream (secondary fluid), propelling it in the process to an intermediate conditions through the partial transfer of momentum (Aidoun *et al.,* 2019). The resulting flow is discharged at a stagnation pressure half way between the primary and secondary pressures. Zhang and Cheng, (2017) carried out a study on combined power and ejector cooling system with R245fa as working fluid. The simulation result showed that a thermal efficiency of 34.1%, an effective efficiency of 18.7% and exergy efficiency of 56.8% could be obtained at a generator temperature of 395K, a condensing temperature of 298K, and an evaporating temperature of 280K. Goudarzi and Taghizadeh, (2023) conducted a study on combined power and ejector refrigeration cycle system for thermal energy recovery from waste heat of internal combustion engine. The study found out that the performance of Rankine-ejector refrigeration system is better than the Rankine-absorption system and the COP is about 51.88% higher.

Yeng *et al,* (2022) carried a study on energy and exergy analysis of cooling/power cogeneration ejector refrigeration system (CPC-ER) and compared it with conventional ejector refrigeration system (CER). The study found out that, the CPC-ER has the higher energy utilization efficiency than the CER system and is suitable for cooling and power in low grade thermal sources. Kheiri *et al* (2017) carried out a thermodynamic modeling and performance analysis of four different configurations of an ORC system. ORC integrated with an ejector (EORC), ORC combined with regenerator (ERORC), ORC integrated with ejector, feed fluid heater (EFFHORC) and ORC integrated with ejector, regenerator and feed fluid heater (ERFFHORC). The results demonstrate that, through the state-of-art modifications, the thermal efficiency of the EORC, ERORC, EFFHORC and ERFFHORC were improved by 13.21%, 15.30%, 18.35% and 19.29% respectively compared with that of simple ORC. The results also show that Cis2-Butame and R245fa had the highest overall power output and thermal efficiency from the operational refrigerants used for all the adopted cycles. The ERFFHORC and the generic ORC operated with R245fa had the maximum and minimum thermal efficiencies respectively. Abam *et al,* (2018a) conducted an exergy analysis of a novel low heat recovery organic Rankine cycle (ORC-NOV) and compared it with an organic Rankine cycle turbine bleeding and regeneration (ORCTBR) system. The

study found out that at base condition, the maximum efficiency of about 7.2% was achieved with ORC-NOV and showed an improved performance of approximately 2% in the turbine output power. Abam *et al,* (2018b) carried out a study on the performance and thermo-suitability analysis of non-hybrid organic Rankine cycle (ORC) at varying heat source and evaporator conditions. The result indicated a high exergetic sustainability index (ESI) and low waste heat ratio (WER) in ORC-IHE and the ORC-TBR for all variations in evaporator pressure and heat source temperature (HST). Ghaebi *et al,* (2017) carried out a study on the performance characteristics of a basic ejector expansion combined cooling and power cycle (EECCPC) and compared it with a three modified EECCPC. EECCPC with turbine bleeding, EECCPC with regenerator and EECCPC with both turbine bleeding and regenerator using R123, R245fs, and Isobutane as refrigerants. The study indicates that the thermal efficiency, overall exergy destruction ration and exergy efficiency can be improved by 24.5, 32 and 72% respectively. Also, selecting R123/Isobutane working fluids for the combined system incorporated with turbine bleeding and recuperator was most appropriate.

These findings are particularly interesting as it confirms the role of an ejector as a crucial important component whose losses must be considered with care in order to achieve high overall system efficiency. In summary, there is little doubt that the incorporation of an ejector into the ORC system gives rise to an interesting and versatile power and cooling technology which has the potential to play an important role in addressing the global energy challenge. In view of the above, this research work objective is aimed at modifying an ORC system to producing power and cooling with simple configurations and reduced components, analyzing its thermodynamic performance and evaluating the system components lifecycle environmental implications which is absent in previous studies.

2. METHODOLOGY

2.1. Process Description

Figure 1 shows the schematic diagram of the energy system for power and cooling. The system consists of an ORC and Ejector Refrigeration Cycle (ERC), with only solar energy as the heat source. The system comprises a vapor generator, turbine, an ejector, a pump, a throttling valve, an evaporator and a condenser. The system is driven by a solar heat energy in which the collector reflects the incident solar radiation on to the focal line towards a receiver that absorbs the concentrated solar energy to raise the temperature of the fluid inside the receiver tube. This high temperature fluid inside the receiver tube then transfers its thermal energy to the refrigerant passing through the heat recovery vapor generator (HRVG).

The cycle starts at point (10) where liquid refrigerant is pumped into the HRVG (10-3) in which the pressure is increased by the pump. The super-heated refrigerant vapor (4) expands in the turbine to drive a coupled generator for power generation. At the turbine (5), a part of the working fluid is bled out which passes through the converging diverging supersonic nozzle of the ejector. The very high velocity refrigerant vapour at the exit of the nozzle creates a very high vacuum at the inlet of the mixing chamber and entrains a secondary vapour from the evaporator (12) into the ejector chamber. The extracted primary vapour (5) and secondary vapour (12) are then mixed in the mixing chamber. The stream (6) out of the ejector which mixes with the turbine exhaust (13) now enters into the condenser (7-8) where it condenses and converted into saturated liquid. At this point, the saturated liquid (8) is divided into two parts (9, 10); one part (9) passes through a throttling valve (TV) where the pressure is reduced to evaporator pressure (11) and feeds into the evaporator. The low temperature and pressure of the working fluid that entered into the evaporator vaporizes (11-12) to produce cooling. The second part of the saturated liquid (10) is pumped into the HRVG where the pump increases its pressure to start a new cycle.

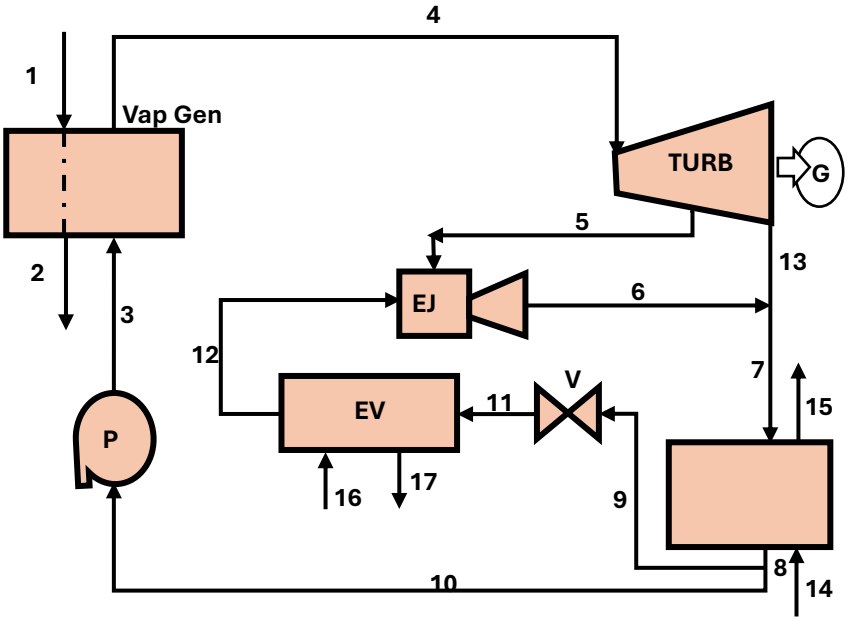

Figure 1: Schematic diagram of an organic Rankine power-cooling cycle

2.2. Thermodynamic Modeling of the System

The modeling involves the development of energy and exergy balance across the components to obtain the necessary thermodynamic properties needed to establish several performance indices in the system. The general energy and exergy balances for any component, *k*, is obtained using the expressions:

$$\dot{Q} - \dot{W} = \sum \dot{m}_0 h_0 - \sum \dot{m}_i h_i \tag{1}$$

$$\sum \dot{m}_\iota \dot{e_\iota} + \dot{E}_Q = \sum \dot{m}_o e_o + \dot{E}_W + \dot{E}_D \tag{2}$$

Where the heat rate is Q, work across the system boundary is W, the mass influx is $\dot{m}_i$, and mass efflux is $\dot{m}_0$. The specific exergy influx, e_i, efflux, e_o, the exergy of heat, $\dot{E}_Q$, and work, $\dot{E}_W$, as well as the exergy destruction, $\dot{E}_D$, in the $\boldsymbol{k}^{\text{th}}$ component are also similarly represented.

Furthermore, for a specific component, the exergy destruction can be expressed in terms of product and fuel (Ifaei *et al.,* 2016; Roy and Ghosh, 2017).

$$\dot{E}_{D,k} = \dot{E}_{F,k} - \dot{E}_{Pk-}\dot{E}_{L,k} \tag{3}$$

The exergy efficiency, ψ_k, the exergy destruction and exergy loss ratios are equally defined for kth component, as in Equations 4 to 6

$$\psi_k = \frac{\dot{E}_{Pk}}{\dot{E}_{F,k}} = 1 - \left[\frac{\dot{E}_{D,k}+\dot{E}_{L,k}}{\dot{E}_{F,k}}\right] \tag{4}$$

$$Y_{D,k} = \frac{\dot{E}_{D,k}}{\dot{E}_{F,total}} \tag{5}$$

$$Y_{L,k} = \frac{\dot{E}_{L,k}}{\dot{E}_{F,total}} \tag{6}$$

Where $\dot{E}$, D, P, L F, and K connote exergy rate, destruction, product, loss, fuel and component. From Equations 1 and 2, the total energy and exergy balances, as well as the exergy efficiencies and destructions are tabulated in Tables 1 and 2.

Table 1: Summary of the energy balance equation

Component	Energy balance equation
Vapour generator	$\dot{m}_g h_1 - \dot{m}_g h_2 = \dot{m}_4 h_4 - \dot{m}_3 h_3$
Turbine	$W_{ORCT} = mg(h_4 - h_5) mg(1 - E_r)(h_5 - h_{13})$
Valve	$\dot{m}_9 h_9 = \dot{m}_{11} h_{11}$
Condenser	$\dot{Q}_{Cond.} = \dot{m}_7 (h_7 - h_8)$
Evaporator	$\dot{Q}_{Evap.} = \dot{m}_{11} (h_{11} - h_{12})$
Ejector	$\dot{m}_{12} h_{12} + \dot{m}_5 h_5 = \dot{m}_6 h_6$
Pump	$\dot{W}_{ORC_{Pump}} = \dot{m}_{10} (h_3 - h_{10})$

Table 2: Equations describing exergy parameters for the system

Components	Exergy flow rate of product ($\dot{E}_{P,k}$)	Exergy flow rate of fuel ($\dot{E}_{F,k}$)	Exergy efficiency (ψ_k)	Exergy balance	Exergy destruction ($\dot{E}_D$)
Vapour generator	$\dot{E}_4 - \dot{E}_3$	$\dot{E}_1 - \dot{E}_2$	$\frac{\dot{E}_4 - \dot{E}_3}{\dot{E}_1 - \dot{E}_2}$	$\dot{E}_1 + \dot{E}_3 + \dot{E}_D = \dot{E}_4 + \dot{E}_2$	$\dot{E}_D = \dot{E}_4 + \dot{E}_2 - \dot{E}_1 - \dot{E}_3$
Turbine	$\dot{W}_t$	$\dot{E}_4 - \dot{E}_5 - \dot{E}_{13}$	$\frac{\dot{W}_t}{\dot{E}_4 - \dot{E}_5 - \dot{E}_{13}}$	$\dot{E}_4 + \dot{E}_D = W_T + \dot{E}_5 + \dot{E}_{13}$	$\dot{E}_D = W_T + \dot{E}_5 + \dot{E}_{13} - \dot{E}_4$
Valve	$\dot{E}_{11}$	$\dot{E}_9$	$\frac{\dot{E}_9}{\dot{E}_{11}}$	$\dot{E}_9 + \dot{E}_D = \dot{E}_{11}$	$\dot{E}_D = \dot{E}_{11} - \dot{E}_9$
Condenser	$\dot{E}_{15}$ - $\dot{E}_{14}$	$\dot{E}_7 - \dot{E}_8$	$\frac{\dot{E}_{15} - \dot{E}_{14}}{\dot{E}_7 - \dot{E}_8}$	$\dot{E}_7 + \dot{E}_{14} + \dot{E}_D = \dot{E}_8 + \dot{E}_{15}$	$\dot{E}_D = \dot{E}_8 + \dot{E}_{15} - \dot{E}_7 - \dot{E}_{14}$
Evaporator	$\dot{E}_{11}$ - $\dot{E}_{12}$	$\dot{E}_{16} - \dot{E}_{17}$	$\frac{\dot{E}_{11} - \dot{E}_{12}}{\dot{E}_{16} - \dot{E}_{17}}$	$\dot{E}_{11} + \dot{E}_{16} + \dot{E}_D = \dot{E}_{12} + \dot{E}_{17}$	$\dot{E}_D = \dot{E}_{12} + \dot{E}_{17} - \dot{E}_{11} - \dot{E}_{16}$
Ejector	$\dot{E}_6$	$\dot{E}_5 + \dot{E}_{12}$	$\frac{\dot{E}_6}{\dot{E}_5 + \dot{E}_{12}}$	$\dot{E}_5 + \dot{E}_{12} + \dot{E}_D = \dot{E}_6$	$\dot{E}_D = \dot{E}_6 - \dot{E}_5 - \dot{E}_{12}$
Pump	$\dot{E}_3 - \dot{E}_{10}$	$\dot{W}_P$	$\frac{\dot{E}_3 - \dot{E}_{10}}{\dot{W}_P}$	$\dot{E}_{10} + \dot{E}_D = \dot{E}_3 + \dot{W}_P$	$\dot{E}_D = \dot{E}_3 + \dot{W}_P - \dot{E}_{10}$

An ejector is a type of pump that uses the Venturi effect of a converging–diverging nozzle to convert the mechanical energy (pressure) of a motive fluid to kinetic energy (velocity), creating a low-pressure zone that draws in and entrains a suction fluid. After passing through the throat of the injector, the mixed fluid expands and the velocity is reduced, recompressing the mixed fluids by converting velocity back to pressure. The process occurring in the ejector is assumed to be under steady state, one dimensional and adiabatic and no work is done during the process as shown in Figure 2. The energy balance in the ejector can be expressed as in Equation (7).

$$\dot{m}_{12} h_{12} + \dot{m}_5 h_5 = \dot{m}_6 h_6 \tag{7}$$

At the inlet and outlet of the ejector the velocities can be considered negligible (Wang and Dia, 2009). In this study, the primary motive flow enters the ejector at point 5 and the suction flow exits the evaporator at point 12. The process in the ejector includes the expansion of the high-pressure prime motive flow through the nozzle, mixing with the low pressure secondary flow in the mixing section at constant pressure and diffusing to the outlet of the ejector (point 6) while the kinetic energy of the mixture is converted to a pressure head as shown in Figure 1. An important parameter for the secondary flow is the entrainment ratio, defined in Equation 8.

$$\omega = \frac{\dot{m}_{12}}{\dot{m}_5} \tag{8}$$

In the nozzle section, the inlet velocity of the primary flow $V_{pf,n1}$ is negligible, so the exit enthalpy and velocity of primary flow can be expressed in Equation 9.

$$V_{pf,n2} = \sqrt{2\eta_{Noz}|h_{pf,n1} - h_{pf,n2,s}|} \tag{9}$$

Nozzle efficiency:

$$\eta n = \frac{h\dot{p}f_1\ \dot{n}_1 - h\dot{p}f_1\ \dot{n}_2}{h\dot{p}f_1\ \dot{n}_1 - h\dot{p}f\dot{n}_{2,s}} \tag{10}$$

Where $h_{pf,n1}$ is the enthalpy at point 5 and $h_{pf,n2,s}$ is the exit enthalpy of the primary flow under isentropic expansion and η_{Noz} is the nozzle efficiency.

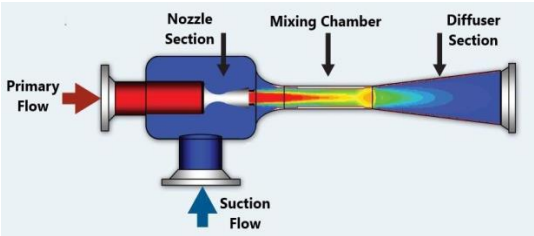

Figure 2: Schematic diagram of an ejector system

Momentum conservation equation for the mixing chamber area gives the following relationship in Equation 11.

$$\dot{m}_5 V_{pf,n2} + \dot{m}_{12} V_{sf,n2} = |\dot{m}_5 + \dot{m}_{12}| V_{mf,m,s} \tag{11}$$

Neglecting the secondary flow velocity $V_{sf,n2}$ compared to the primary flow velocity $V_{pf,n2}$, the exit velocity of mixed flow $V_{mf,m,s}$ can be expressed as in Equation 12.

$$V_{mf,m,s} = \frac{V_{pf,n2}}{1+\omega} \tag{12}$$

The mixing chamber efficiency can be expressed as in Equation 13.

$$\eta_{Mix} = \frac{V_{mf,m}^2}{V_{mf,ms}^2} \tag{13}$$

Therefore, the actual velocity of the mixed flow is expressed as in Equation 14

$$V_{mf,m,s} = \frac{V_{pf,n2}\sqrt{\eta_{Mix}}}{V_{mf,ms}^2} \tag{14}$$

The energy equation for the mixing chamber is expressed in Equation 15

$$\dot{m}_5 \left| h_{pf,n2} + \frac{V_{pf,n_2}^2}{2} \right| + \dot{m}_{12} \left| h_{sf,n_2} + \frac{V_{sf,n_2}^2}{2} \right| = \dot{m}_6 \left| h_{mf,m} + \frac{V_{mf,m}^2}{2} \right| \tag{15}$$

By simplifying Equation 15 and using Equations. (8) and (14), the enthalpy of mixed flow is obtained in Equation 16.

$$h_{mf,m} = \frac{h_{pf,n_1} + \omega h_{sf,n_2}}{1+\omega} - \frac{V_{mf,m}^2}{2} \tag{16}$$

In the diffuser section, the mixed flow converts its kinetic energy to a pressure increase. Assuming the exit velocity of the mixed flow to be negligible and considering the diffuser efficiency, the actual exit enthalpy of the mixed flow is calculated as in Equation 17

$$h_6 = h_{mf,m} + \left|h_{mf,ds} - h_{mf,m}\right|/\eta_{Dif} \quad (17)$$

Diffuser efficiency is as in Equation 18.

$$\eta_d = \frac{h_{mf,d,s} - h_{mf,m}}{h_{mf,d} - h_{mf,m}} \quad (18)$$

Where $h_{mf,ds}$ is the ideal exit enthalpy of the mixed flow with isentropic compression, and η_{Dif} is the diffuser efficiency. Using these equations, the entrainment ratio is expressed as (Wang and Dia, 2009) in Equation 19

$$\omega = \sqrt{\eta_{Noz}\eta_{Mix}\eta_{Dif}\left|\frac{h_5 - h_a}{h_{13} - h_b}\right|} - 1 \quad (19)$$

Where η_{Noz}, η_{Mix}, η_{Dif} are the nozzle, mixing chamber and diffuser efficiencies.

2.3. Life Cycle Analysis of the System

The life cycle analysis (LCA) of the system comprises different stages: the construction, operation and decommissioning stages. For the system, the LCA boundary is defined by the system components; vapour generator, turbine, condenser, pump, evaporator, the ejector and the working fluid. The influence of the piping system and connecting devices such as valve, temperature gauges and couplings are not considered as well as their effect on the environment. Additionally, the working fluid interaction with the environment exist at the three stages of development of the system indicated as: the production stage, the operation stage, where seepage occurs and the decommissioning stage, where there is emission due to the loss in mass of the working fluid which escapes to the environment (Zhang *et al.,* 2014). On the contrary, during the system design the effect of the working fluid interaction with the environment is taken into account as the working fluid may trickle to the environment especially at the operation stage owing to failures in joint seals, valves seals and pipe deterioration predominantly caused by corrosion. Consequently, in the development of the LCA, exergy model or exergoenvironmental model, working fluid seepage is factored into the model. Studies have indicated such seepages value to range between 0 and 2 % which in practice, the percentage loss is multiplied by the design operating years of the plant to obtained the actual loss of the working fluid to the original value (Zhang and Cheng, 2017; Gerber and Marechal, 2012). Another consideration factored into the model is the emission loss and the waste oil during the discharge of the non-condensate at the decommissioning stage. This loss should not be less than 3 % of the overall working fluid recovered in the recovering process, which is adopted in this study (ARI 740 - 98). For the component system, the Eco-indicator 99 procedure is applied to compute the effect of each component on the environment (Goedkoop *et al.,* 2001).

2.3.1 Calculation of the component masses

The total area of the heat transfer of the kth component is calculated in Equation 20 (Song et al. 2016).

$$A_k = \frac{\dot{Q}_k}{U_k \Delta T_k} \quad (20)$$

Where:

$\dot{Q}_k$ = Rate of heat transfer ((kW), A_k = Heat transfer area (m^2), U_k = Coefficient of heat transfer $(W/m^2.K)$, ΔT_k = Logarithmic mean temperature difference expressed as (Song *et al.,* 2016) in equation 21

$$\Delta T_k = \frac{\Delta T_{kmax} - \Delta T_{min}}{\ln \frac{\Delta T_{kmax}}{\Delta T_{kmin}}} \quad (21)$$

The condenser and evaporator masses are calculated from (Liu *et al*., 2013) expressed in Equation 22.

$$M_k = \rho \times A_k \times \delta \tag{22}$$

Where $\rho, A_k, and\ \delta$ are density, area and thickness of the k^{th} component.

The pump and turbine masses are calculated from (Fergani *et al.,* 2016; Antipova *et al.,* 2013) in Equation 23.

$$M_k = \alpha \times W_k \tag{23}$$

Where α denotes the material quality and per kW of the turbine power while W_k defines the consumed power of the pump in the generated power of the turbine (kW).

2.3.2. Components' life cycle analysis

The effect of the kth component on the environment is defined in Equation 24.

$$Y_k = \omega_k \times M_k \tag{24}$$

Where ω_k, is the eco-99 coefficient of the kth system component (mPts/kg), while the impact of the $\boldsymbol{k^{th}}$ on the environment and the overall environmental impact for the three stages, construction, operation and decommissioning are calculated using Equation 25 and 26.

$$Y^{LCA} = Y_k^{con} + Y_k^{om} + Y_k^{wf} \tag{25}$$

$$Y_k = Y^{LCA} + Y_k^{wf} \tag{26}$$

The exergoenvironmental description for the system components in Figure 1 is performed in the study of (Meyer *et al.,* 2009). The general exergoenvironmental balance equations for $\boldsymbol{k^{th}}$ component of a system is expressed in Equation 27 and 28

$$\sum \dot{B}_{out} = \sum \dot{B}_{in} + \dot{Y}_k \tag{27}$$

$$\dot{B} = \dot{E} \times b \tag{28}$$

Where $\dot{B}$ is the exergoenvironmental impact rate (mPts/h), $\dot{Y}_k$ is the environmental impact rate of the $\boldsymbol{k^{th}}$ component (mPts/h),$\dot{E}$ is the rate of exergy flow (kW) and b is the specific impact on the environment (mPts/GJ) calculated for both product and fuel as presented in Equation 29 and 30. Similarly, the environmental impact due to exergy destruction is calculated in Equation 31.

$$b_{Pk} = \frac{\dot{B}_{P,k}}{\dot{E}_{P,k}} \tag{29}$$

$$b_{Fk} = \frac{\dot{B}_{F,k}}{\dot{E}_{F,k}} \tag{30}$$

$$\dot{B}_{D,k} = b_{F,k} \times \dot{E}_{D,k} \tag{31}$$

Furthermore, the exergoenvironmental impact equations $(\dot{B})$, the environmental impact rate ($\dot{Y}_k$) of the $\boldsymbol{k^{th}}$ component is presented in Table 3.

2.3.3. Exergoenvironmental evaluation for the refrigerant (working fluid)

The impact of the refrigerant or working fluid is not enveloped in the exergoenvironmental model of the organic Rankine cycle. On this, allocation rule has been applied (Fergani *et al*., 2016) where the environmental effect of the working fluid is described. The latter is achieved by assigning the exergoenvironmental effect of the working fluid to respective components of the system based on the percentage of exergy destruction of the respective components expressed in Equation 32.

$$Y_k^{wf} = y_{D,k}^{*} \times Y_{wf} \tag{32}$$

Where Y_{wf} is the total impact of the working fluid on the environment, $y^*_{D,k}$ is the ratio of exergy destruction. The overall impact of the working fluid on the environment is obtained using Equation 33.

$$Y_{wf} = Y_{wf}^{con} + Y_{wf}^{om} + Y_{wf}^{dec} \tag{33}$$

Where Y_{wf}^{con}, Y_{wf}^{om}, $and\ Y_{wf}^{dec}$ describes the environmental impact due to the working fluid at stages of construction, maintenance and, operation and decommissioning, respectively. Additionally, during the operation stage seepage of working fluid occurs and this is measured by Equation 34.

$$M_{wf}^{yl} = M_{wf} \times \beta \times n \tag{34}$$

Where M_{wf}^{yl}, is quantity of working fluid leakage (kg), M_{wf} is the working fluid quantity filled during the operation stage, β is the annual leakage proportion of fluid (%) and n is the plant years.

Table 3: Exergoenvironmental impact equation of the energy system

Component	Exergoenvironmental impact equation	Auxiliary equation
Vapour generator	$\dot{B}_1 + \dot{B}_3 + \dot{Y}_{vg} = \dot{B}_{2+}\dot{B}_4, \dot{Y}_{vg} = \frac{Y_{vg}}{(\tau \times n)}$	$\frac{\dot{B}_1}{\dot{E}_1} = \frac{\dot{B}_2}{\dot{E}_2}$
Turbine	$\dot{B}_4 + \dot{Y}_{tub} = \dot{B}_5 + \dot{B}_{13} + \dot{B}_{wt}\dot{Y}_{tub} = \frac{Y_{tub}}{(\tau \times n)}$	$\frac{\dot{B}_4}{\dot{E}_4} = \frac{\dot{B}_5}{\dot{E}_5}$ $\frac{\dot{B}_5}{\dot{E}_5} = \frac{\dot{B}_{14}}{\dot{E}_{13}}$
Valve	$\dot{B}_9 + \dot{Y}_{val,} = \dot{B}_{11}, \dot{Y}_{val} = \frac{Y_{val}}{(\tau \times n)}$	$\frac{\dot{B}_9}{\dot{E}_9} = \frac{\dot{B}_{11}}{\dot{E}_{11}}$
Condenser	$\dot{B}_7 + \dot{B}_{14} + \dot{Y}_{con} = \dot{B}_8 + \dot{B}_{15}, \dot{Y}_{con} = \frac{Y_{con}}{(\tau \times n)}$	$\frac{\dot{B}_7}{\dot{E}_7} = \frac{\dot{B}_8}{\dot{E}_8}$
Evaporator	$\dot{B}_{11} + \dot{B}_{16} + \dot{Y}_{evp} = \dot{B}_{12} + \dot{B}_{17}, \dot{Y}_{evp} = \frac{Y_{evp}}{(\tau \times n)}$	$\frac{\dot{B}_{16}}{\dot{E}_{16}} = \frac{\dot{B}_{17}}{\dot{E}_{17}}$
Ejector	$\dot{B}_5 + \dot{B}_{12} + \dot{Y}_{EJCT} = \dot{B}_6\ , \dot{Y}_{Eje} = \frac{Y_{EJCT}}{(\tau \times n)}$	$\frac{\dot{B}_5}{\dot{E}_5} = \frac{\dot{B}_6}{\dot{E}_6}$ $\frac{\dot{B}_5}{\dot{E}_5} = \frac{\dot{B}_{12}}{\dot{E}_{12}}$
Pump	$\dot{B}_{10} + \dot{Y}_{pum} + \dot{B}_{wp} = \dot{B}_3\ , \dot{Y}_{pum} = \frac{Y_{pum}}{(\tau \times n)}$	$\frac{\dot{B}_{10}}{\dot{E}_{10}} = \frac{\dot{B}_3}{\dot{E}_3}$

Similarly, during decommissioning, the emission of the fluid due to the discharge of non-condensate gas is evaluated using Equation 35.

$$M_{wf}^{em} = \left(M_{wf} - M_{wf}^{yl}\right) \times \gamma \tag{35}$$

Where: M_{wf}^{em} = quantity of emitted working fluid during decommissioning (kg) and γ = the working fluid emission ratio (%).

2.4. Performance Validation

The result from the study is validated and compared with related theoretical basic combined power-cooling cycle integrated with an ejector system using same operating parameters. The turbine output, evaporator cooling rate, energy and exergy efficiency was compared with the work of Ghaebi *et al.,* (2017). The research was the closest in system configuration to the present work. The result shows

significant improvement using R245fa as the common refrigerant. An improvement potential (IP) was obtained in the power output of about 36.26% while the efficiencies followed the same improvement trend with about 48.2% improvement potential in the evaporator cooling rate. The validation performance is shown in Table 4.

Table 4: Performance validation of the EORPCC

Parameters	Ghaebi *et al. (*2017)	Current work	Improvement Potential
Turbine output (KW)	15.64	24.54	8.9
Energy efficiency (%)	14.47	37.57	23.1
Exergy efficiency (%)	35.87	41.46	5.59
Evaporator cooling rate (KW)	17.02	32.87	15.85
Refrigerant	R245fa	R245fa	
Mass flow rate (kg/s)	0.52	0.52	
Turbine inlet temperature (K)	150	150	

3. RESULTS AND DISCUSSION

3.1. Operating Parameters and Thermodynamic Approach

System properties are presented subject to these thermodynamic assumptions for the three considered refrigerants.

- The ambient temperature and pressure were taken as 27 ºC and 1.013 bar, resectively.
- The lower and upper operating pressures were taken as 4.129 and 18 bar for R245fa. Corresponding values were taken as 6.5 and 18 bar, as well as 4.32 and 18 bar for R1234yf and R1234ze, respectively.
- The turbine inlet temperature were taken as 120 ºC, 100 ºC, and 110 ºC for refrigerants R245fa, R1234yf and R1234ze, resectively.
- The refrigerant mass flow rate was 3 kg/s for all refrigerants and is made subject to the required energy balance around the vapour generator.
- The system was analyzed at steady state conditions with the effect of pressure and temperature drops neglected.
- The system boundaries were treated as adiabatic such that the heat losses to the surroundings were neglected.
- The effect of valve and ejector has been neglected in the life cycle analysis.

The thermodynamic simulation results from the three refrigerants are shown in Tables 4, 5, and 6 for R245fa, R1234yf and R1234ze, respectively. The plant operating hours for one year was taken as 7000 h while the lifetime operating hours (n) was 20 years. These parameters with the operating data were used to develop codes in engineering equation solver (EES) for the system in order to generate the thermodynamic flow parameters for the different working fluids. The input parameters for all the refrigerants were taken as 350 K while the highest exergy flow rate was obtained at 366.40 KW with R1234ze as shown in Table 7. For refrigerant R245fa and R1234yf, the exergy flow rates for these fluids are with values of 364.30 and 332.7 KW as shown in Tables 5 and 6 respectively. However, the entropy changes within the working fluids were found to vary across the components and these variations across the refrigerants and components must have been responsible for the decline in the exergy flow rates.

3.2. Performance Index of the Plant

The measured performance index includes the system heat input, turbine output, pump work, evaporator cooling rate, total energy and exergy efficiencies. Within the indicated performance

indicators, a comparative analysis between the energy and exergy efficiency, turbine output and evaporator cooling rate is shown in Table 8. The ORC system configuration has a relatively high energy and exergy efficiencies (up to 34.43 %, 28.87 %, and 32.28 % energy efficiencies for R245fa, R1234yf, and R1234ze, respectively). The performance also shows an exergy efficiency of 25.7, 31.27 and 31.68% for R245fa, R12384yf and R12384ze respectively. This enhancement is due to the additional cooling provided by the ejector refrigeration system (ERS). The additional product by virtue of the ERS is 151.9, 120.8, and 153 kW for R245fa, R1234yf, and R1234ze, respectively. Evidently, R1234ze and R245fa are thermodynamically better options for running the developed system within the boundaries of the thermodynamic properties developed in the study. Based on the operating data for the system, the pump work was nearly the same at 3.33, 3.142, and 3.486 kW, for R245fa, R1234yf, and R1234ze, respectively.

Table 5: Thermodynamic simulation data at the state points for R245fa

State	Temperature [ºC]	Pressure [Bar]	Enthalpy [kJ/kg]	Entropy [kJ/kg.K]	Mass [kg]	Energy [kW]
1	350.00	1.013	631.50	6.448	3.40	364.30
2	150.00	1.013	424.60	6.048	3.40	28.64
3	40.60	18.000	235.50	1.178	3.0	28.64
4	120.00	18.000	487.90	1.811	3.0	162.30
5	90.00	7.991	473.20	1.811	1.20	47.25
6	65.90	5.434	452.10	1.771	2.20	66.49
7	66.20	4.129	455.90	1.797	4.00	104.70
8	40.00	4.129	252.40	1.178	1.00	8.48
9	40.00	4.129	252.40	1.178	1.00	8.48
10	40.00	4.129	252.40	1.178	3.00	25.43
11	30.60	1.800	252.40	1.179	1	8.11
12	30.60	1.800	426.80	1.754	1.00	10.12
13	70.50	4.129	460.50	1.811	1.80	48.11
14	20.00	1.013	83.30	0.294	12.97	0.00
15	35.00	1.013	146.00	0.503	12.97	1.19
16	27.00	1.013	300.40	5.702	6.68	0.00
17	1	1.013	274.30	5.611	6.68	8.02

Table 6: Thermodynamic simulation data at the state points for R1234yf

State	Temperature [ºC]	Pressure [Bar]	Enthalpy [kJ/kg]	Entropy [kJ/kg.K]	Mass [kg]	Energy [kW]
1	350.00	1.013	631.5	6.448	3.103	332.7
2	150.00	1.013	424.6	6.048	3.103	62.61
3	24.20	18	232.9	1.114	3	119.2
4	100	18	447	1.75	3	188.8
5	70.00	7.211	426.8	1.75	1.2	51.38
6	47.10	12.08	393.1	1.617	2.2	108
7	50.50	6.5	407.3	1.698	4	155.4
8	23.4	6.5	231.9	1.111	1	39.73
9	23.4	6.5	231.9	1.111	1	39.73
10	23.4	6.5	231.9	1.121	3	119.2
11	-15.4	1.8	231.9	1.126	1	35.07
12	-15.4	1.8	352.7	1.595	1	15.18
13	66.9	6.5	424.5	1.75	1.8	72.9
14	20	1.013	83.3	0.294	11.18	0
15	35	1.013	146	0.5029	11.18	1.022
16	27	1.013	300.4	5.702	4.627	0
17	1	1.013	274.3	5.611	4.627	5.558

Table 7: Thermodynamic simulation data at the state points for R1234ze

State	Temperature [°C]	Pressure [Bar]	Enthalpy [kJ/kg]	Entropy [kJ/kg.K]	Mass [kg]	Energy [kW]
1	350	1.013	631.5	6.448	3.418	366.4
2	150	1.013	424.6	6.048	3.418	68.96
3	20.9	18	226.7	1.09	3	104.6
4	110	18.000	462.5	1.779	3	191.2
5	85.0	9.306	447.6	1.779	1.2	58.59
6	69.3	15.8	416.2	1.659	2.2	118
7	51.5	4.32	422.5	1.756	4	123.1
8	20.4	4.32	225.6	1,09	1	33.72
9	20.4	4.32	225.6	1.09	1	33.72
10	20.4	4.32	225.6	1.09	1	33.72
11	-5	1.8	225.6	1.096	1	31.91
12	-5	1.8	378.6	1.667	1	13.68
13	59.7	4.32	430.2	1.779	1.8	56.6
14	20	1.013	83.3	0.294	12.56	0
15	35	1.013	146	0.5029	12.56	1.147
16	27.0	1.013	300.4	5.702	5.862	0
17	1	1.013	274.3	5.611	5.862	7.041

In terms of net power output from the expander with same refrigerant mass flow, as much as 75 kW was obtained with R1234ze, while the other refrigerants gave about 65 kW. The evaporator cooling rate was also high with R1234ze. However, the highest exergy efficiency for the system was obtained when run with R245fa. This is attributable to the enthalpy properties of R245fa by virtue of the energy balance around the vapour generator.

Table 8: Performance indicators of the plant

Performance index	Value			Unit
	R245fa	R1234yf	R1234ze	
System heat input	635.8	642.1	707.2	kW
Turbine output	66.98	64.57	75.98	kW
Pump work	3.332	3.142	3.486	kW
Evaporator cooling rate	151.9	120.8	153	kW
System exergy efficiency	25.7	31.27	31.68	%
System energy efficiency	34.43	28.87	32.38	%

3.3. LCA and Exergoenvironmental Analysis of the System Plant

The LCA method was used for computation of the environmental impacts of the components. The leakage of working fluid to the atmosphere was also considered in the analysis. During the leakage to the atmosphere, the Eco 99 coefficients were approximated as 7300, 19654, and 674 mPts/kg for R1234ze, R1234yf, and R245fa, respectively (Goedkoop *et al.,* 2001). The corresponding Eco 99 coefficients for the manufacturing phase are also taken as 150, 99, and 99 mPts/kg for R1234z4, R1234yf, and R245fa, respectively (Goedkoop *et al.,* 2001).

The working fluids data for the life cycle analysis is presented in Table 9. The filling amount for the refrigerants in the construction phase has been highlighted for the selected working fluids. The filling mass of the working fluid is 5.57 kg and 5.4 kg for a 1-kW power output generated by the turbine (Murillo *et al,* 2020). In this study, a filling mass of the working fluid of 5.57 kg for a 1-kW power output is used. In the operation phase, a 10 per cent leakage was assumed leaving 90 per cent of the filled refrigerants for the operation phase. Furthermore, 3 percent of the leakage quantity was used for the required amount in the decommissioning phase. The corresponding values are shown for R245fa, R1234ze, and R1234yf in Table 8.

Table 9: LCA relative data of working fluid

Phase	Operation	R245fa	R1234ze	R1234yf
Construction phase	Filing quantity	373.0786	359.6549	423.2086
Operation phase	Leakage quantity	37.30786	35.96549	42.32086
Decommissioning phase	Emission loss quantity	10.07312	9.710682	11.42663

The heat transfer rate and the area for such heat transfer in the evaporator, vapour generator and condenser are required for computation of the mass of these components during the construction phase. This is shown in Table 10. Since no material is lost during the operation phase, the mass requirements are neglected. However, in the decommissioning phase, the remainders of the materials of the entire components of the system were taken as 4.5 % of the manufacturing components' masses, respectively. For the refrigerants, their values for the system during construction, operation and decommissioning phases are shown in Table 8.

Table 10: Heat transfer parameters for life cycle analysis

Parameter	R245fa	R1234yf	R245ze
Condenser heat rate (kW)	724.1	701.5	787.8
Condenser Area (m^2)	100.1	119.7	98.0
Vapour generator heat rate (kW)	635.8	642.1	707.2
Vapour generator area (m^2)	112.4	108.4	102.5
Evaporator heat rate (kW)	151.9	120.8	153
Evaporator area (m^2)	16.8	21.2	14.4

Life cycle analysis results for the system using different refrigerants are shown in Tables 11, 12, and 13. Steel was used as the material for the system and the analysis as indicated in the methods covered the construction, operation and decommissioning stages. The life cycle analysis for the working fluids was also considered. The components considered in the analysis include the evaporator, condenser, pump, and turbine. The coefficient of degradation using steel as material for the physical components was taken as 86 mPts/kg and applies to the evaporator, condenser, pump, and turbine during construction, operation and decommissioning phases.

Table 11: R245fa LCA computation results

Component	Material	Degradation coefficient (mPts/kg)	Quality (kg)	Y^{co} (mPts)	Y^{op} (mPts)	Y^{dec} (mPts)	Y (mPts)
Vap. Gen	Steel	86	1782.664	153309.104	0	6898.90	160208.01
Evaporator	Steel	86	266.448	22914.53	0	1031.154	23945.68
Condenser	Steel	86	1587.586	136532.4	0	6143.958	142676.4
Pump	Steel	86	46.648	4011.728	0	180.5278	4192.256
Turbine	Steel	86	2089.776	179720.7	0	8087.433	187808.2
Fluid	R1234ze	150*/7300#	373.0786	55961.79	272347.4	73533.79	401843

*Refrigerant Eco 99 coefficients during manufacturing; #Refrigerants Eco 99 coefficients for operation and decommissioning phases

Table 12: R1234ze LCA computation results

Component	Material	Degradation coefficient (mPts/kg)	Quality (kg)	Y^{co} (mPts)	Y^{op} (mPts)	Y^{dec} (mPts)	Y (mPts)
Vap. Gen.	Steel	86	1625.65	139805.9	0	6291.26	146097.16
Evaporator	Steel	86	228.384	19641.02	0	883.8461	20524.87
Condenser	Steel	86	1554.28	133668.1	0	6015.064	139683.1
Pump	Steel	86	48.804	4197.144	0	188.8715	4386.015
Turbine	Steel	86	2370.576	203869.5	0	9174.129	213043.7
Fluid	R1234ze	99*/19654#	359.6549	35605.84	706865.7	190853.7	933325.3

Table 13: R1234yf LCA computation results.

Component	Material	Degradation coefficient (mPts/kg)	Quality (kg)	Y^{co} (mPts)	Y^{op} (mPts)	Y^{dec} (mPts)	Y (mPts)
Vap. Gen.	Steel	86	1719.224	147853.264	0	6653.39	154506.66
Evaporator	Steel	86	336.232	28915.95	0	1301.218	30217.17
Condenser	Steel	86	1898.442	163266	0	7346.971	170613
Pump	Steel	86	43.988	3782.968	0	170.2336	3953.202
Turbine	Steel	86	2014.584	173254.2	0	7796.44	181050.7
Fluid	R1234ze	99*/674#	423.2086	41897.65	28524.26	7701.55	78123.46

In Figure 3, a comparative analysis of the environmental impact of the system components is provided in line with the operating refrigerants. When the performance criteria is of priority, the components with refrigerant R245fa has less environmental impact followed by R1234ze and R1234yf. This is totally attributed to the heat transfer rates, pump power, and turbine power by virtue of the system operation using R245fa and not the environmental friendliness of this fluid which is clearly indicated in Tables 10, 11, and 12. The environmental impact of the refrigerants is shown in Figure 4, computed based on the data in Table 9. The filling mass and the specific environmental impact in milipoints per kilogram are the two driving variables for the total impact from the use of these working fluids. Clearly, as shown in Figure 4, the refrigerant R1234ze has the most environmental impact, with a value totaling 933325.3 mPts. Although this value does not completely connote physical damage related to a known environmental effect, its comparison with similar values represents its potential to impact more on the environment by some chosen index for environmental degradation. Less environmental impact of 78,123.46 mPts was recorded when R1234yf was selected as the working fluid.

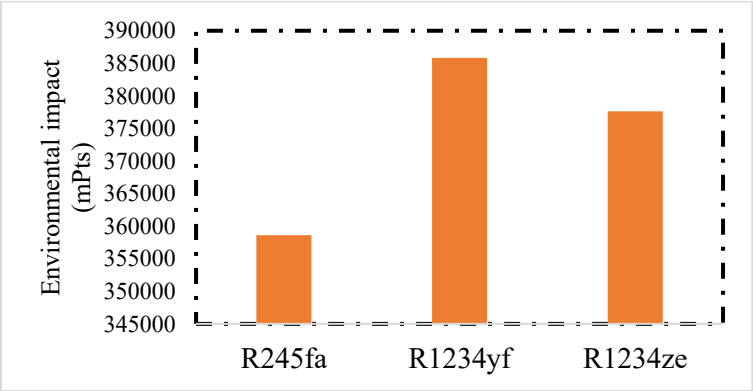

Figure 3: Comparative LCA results for the system with different refrigerants

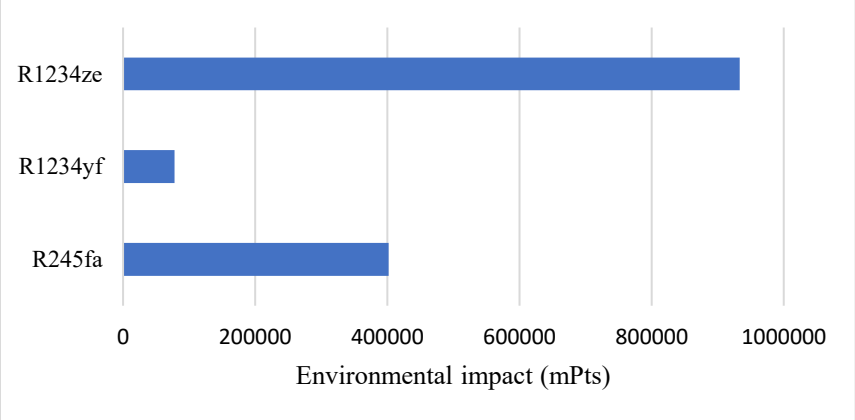

Figure 4: Total environmental impacts from selected working refrigerants in the study

The quantity of environmental impact from the refrigerants is spread between the construction, operation and decommissioning phases with the operation phases accounting for the highest part of the total emissions. This is shown in Figure 5 with R1234ze accounting for up to 3.81, 75.74 and 20.45% respectively, for the construction, operation and decommissioning phases.

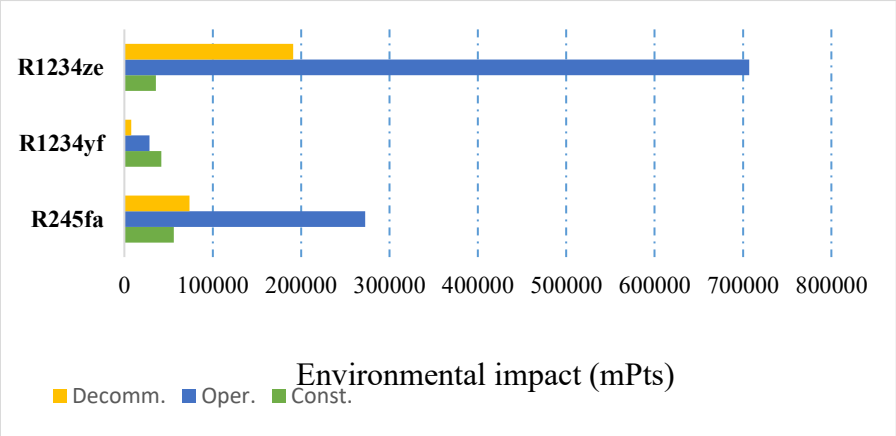

Figure 5: Refrigerant environmental impact during the lifetime of the system

3.4. Sensitivity Analysis of the EORPCC System

An analysis was performed on the sensitivity of the EORPCC to evaluate the variables that affects the performance of the system. The exergy destruction (ED) inceases with an increase in evaporator pressure (EVPP). The highest values of ED was obtained at EVPP of 4.0bar at 159kw, 175kw and 185kw for R1234yf, R1234ze and R245fa respespectively. The lowest values of ED was obtained at 108kw, 124kw and 156kw for R1234yf, R1234ze and R245fa respectively as shown in Figure 6 for the different working fluids. The cooling rate decreases with an increase in turbine back pressure (TBP) between 1.2 and 4.0bar. The cooling rate decreases from 185kw to 144kw for R1234yf. It also decreases from 201kw to 158kw and 202kw to 153kw for R1234ze and R245fa respectively as shown in Figure 7a. The increase in ejector mass flow rate (EMR) increases the cooling rate. The highest values of cooling rate between 1.0kg/s to 1.76kg/s occurred at 215kw, 268kw and 268.04kw for R1234yf, R1234ze and R245fa respectively as indicated in Figure 7b. At constant pressure, the effect of increasing the turbine inlet temperature (TIT) increases the enthalpy of the expanding gasses, thereby increasing both the turbine output and the cycle efficiency. The result demonstrates a linear increment in turbine output and efficiency with increasing turbine inlet temperature as shown in Figure 8.

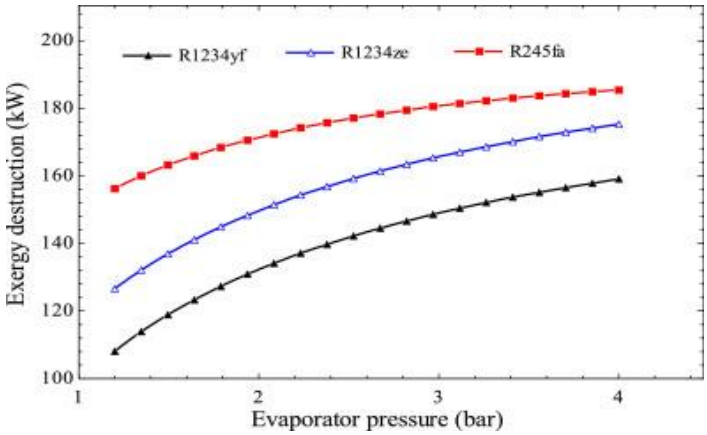

Figure 6: Effect of evaporator pressure on exergy destruction

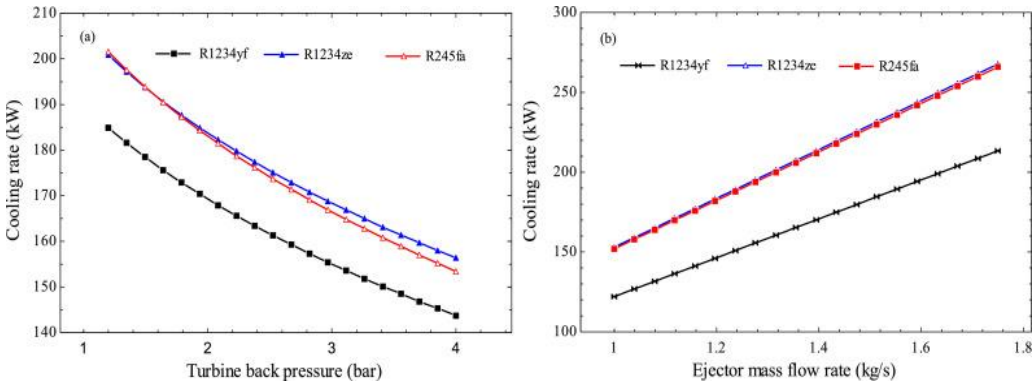

Figure 7a: Effect of (a) TBP and (b) EMR on cooling rate

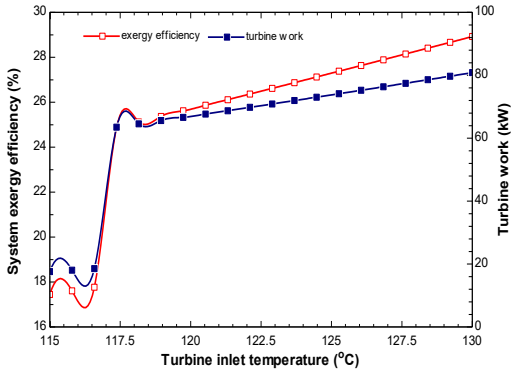

Figure 8: Effect of TIT on power output and efficiency

Figure 9a and 10b shows the effect of turbine back pressure (TBP) and ejector mass flow rate (EMR) on the unit cost of electricity. Increasing the TBP increases the UCOE for all the working fluids. The minimum UCOE occurred at 0.128 $/kw, 0.142 $/kw and 0.162 $/kw for R1234ze, R1234yf and R245fa respectively as shown in Figure 9a. Similarly, increasing EMR decreases the UCOE. The least UCOE (0.123 $/kw) occurred with R1234ze at EMR of 1.75kg/s while R1234yf and R245fa had similar UCOE of 0.156$/kg at 1.76kg/s EMR shown in Figure 9b.

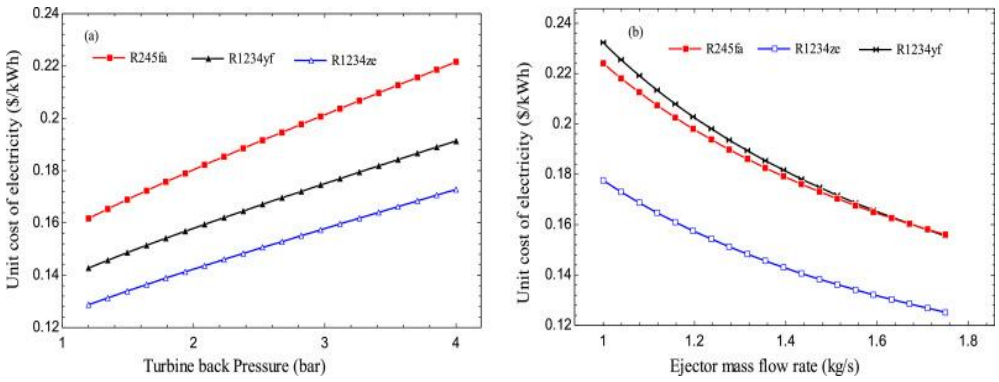

Figure 9a: Effect of (a) TBP and (b) EMR on UCOE

4. CONCLUSION

This report investigates the exergy-based life cycle analysis of an organic Rankine power-cooling cycle integrated with an ejector system. The system was driven by solar heat energy that is absorbed by the heat transfer fluid inside the receiver tube that transfers its heat content to the organic fluid. The modeling of the solar heat characteristics was limited to its mass flow rate and heat content. Three organic refrigerants - R245fa, R1234yf, and R1234ze - were used for the analysis that covered

thermodynamics and exergy based life cycle analysis concept. The manufacture and leakage of working fluid were considered in the life cycle analysis from the construction, operation and decommissioning phases of the plant. The following major conclusions were drawn:

- The ORC system configuration had a relatively high energy and exergy efficiencies (up to 34.43, 28.87 and 32.28 energy efficiencies while 25.7 31.27and 31.68 exergy efficiencies for R245fa, R1234yf, and R1234ze, respectively). This enhancement was due to the additional cooling provided by the ejector refrigeration system (ERS).
- The additional product by virtue of the ERS was 151.9, 120.8, and 153 kW for R245fa, R1234yf and R1234ze respectively.
- R1234ze and R245fa were thermodynamically better options for running the developed system within the boundaries of the thermodynamic properties developed in the study.
- When the performance criteria was of priority, the system components with refrigerant R245fa had the least environmental impact with a value of 518,831mpts followed by R1234ze and R1234yf with values of 523,735mpts and 540,341mpts respectively. Due to leakages, refrigerant R1234yf had the least environmental impact followed by R245fa and R1234ze. The refrigerant R1234ze had the most environmental impact, with a value totaling 933,325.3mPts. Least environmental impact of 78,123.46 mPts was recorded when R1234yf was selected as the working fluid.
- The operation phase accounts for the highest part of the total emissions with R1234ze accounting for up to 3.81, 75.74 and 20.45% respectively for the construction, operation and decommissioning phases..

5. CONFLICT OF INTEREST

There is no conflict of interest associated with this work.

REFERENCES

Abam, F.I., Tobinson, A. Briggs, Ekwe, B. Ekwe, Kanu, C.G., Samuel, O. Effiom, Ndukwu M.C. (2018a). Exergy analysis of a novel low heat recovery organic Rankine cycle (ORC) for combined cooling and power generation. *Energy sources*, Part A: Recovery, Utilization and environmental Effects. 41(13), pp. 1649- 1662.

Abam, F.I., Ekwe, B., Samuel, F., Samuel, O.E., and Chrystopher, B.A. (2018b). Performance and thermo-sustainability analysis of non-hybrid organic Rankine cycles (ORCs) at varying heat Sources and evaporator conditions. *Australian Journal of Mechanical Engineering*. 16 (3), pp. 238-248.

Aidoun, Z. Ameur, K., Falsafioon, M. and Badache, M. (2019). Current advances in ejector modeling, experimentation and application for refrigeration and heat pumps part 1: simple phase ejectors. *Inventions*, 4, pp. 1-73.

Antipova, E., Boer, D., Cabeza, L.F., Guillén-Gosálbez, G., Jiménez, L. (2013). Multi-objective design of reverse osmosis plants integrated with solar Rankine cycles and thermal energy storage. *Applied Energy*, 102, pp. 1137-47.

Air-conditioning and Refrigeration Institute (ARI 740 – 98). Standard for Refrigerant Recovery and Recycling Equipment.

Fergani, Z., Touil, D., and Morosuk T. (2016). Multi-criteria exergy based optimization of an Organic Rankine Cycle for waste heat recovery in the cement industry. *Energy Conversion and Management,* 112, pp. 81-90.

Goedkoop, M., Effting, S., Collignon, M. (2001). The Eco-indicator 99: A damage oriented method for life-cycle impact assessment. Manual for designers: *Product Ecology Consultants.* 3, pp.53 - 74

Gregory, Casey. (2025). Energy Availability and Economic Growth. *Energy Economics*.149, pp. 0140 - 9883

Gerber, L.and Marechal, F. (2012). Environomic optimal configurations of geothermal energy conversion systems: Application to the future construction of Enhanced Geothermal Systems in Switzerland. *Energy*, 45 (1), pp. 908-23.

Ghaebi, H., Rostamzadeh, Hadi and Pouria, S. Martin (2017). Performance evaluation of Ejector expansion combined cooling and power cycles. *Heat Mass Transfer* 55, pp 2915- 2931.

Goudarzi, K., and Taghizadeh, A.R. (2023). A combined power and Ejector refrigeration cycle system for thermal energy recovery from waste heat of internal combustion engine. *Journal of Energy and Power Technology*. 5(1): pp. 1 - 23

International Energy Agency (IEA) Report, 2025. World Energy Outlook

Ifaei, P., Ataei, A. and Changkyoo, Y. (2016). Thermoeconomic and environmental analysis of a water consumption combined steam power plant and refrigeration chillers part 2. *Energy Conversion and Management*. 123, pp. 610 - 624

Ihim, U.J., Sabiu, S.B. (2023). Energy consumption on environmental pollution and economic growth in Nigeria. International Research Journal of Economics and Management Studies. 2(3), pp. 653 - 662

Kheiri, R., Hadi, G., Mohammad, E., Rostamzadeh, H. (2017). Thermodynamic modeling and performance analysis of four new integrated organic Rankine cycle (A comparative study). *Applied Thermal Engineering.* 122, pp. 103-117

Kolahi, M., Yari, M. and Mahmoudi, S. M. S. (2016). Thermodynamic and economic performance improvement of ORCs using zeotropic mixtures: Case of waste heat recovery in an offshore platform. *Case Studies in Thermal Engineering*. 8, pp. 51-70

Liu, C., He, C., Gao, H., Xie, H., Li, Y., Wu, S. (2013).The environmental impact of organic Rankine cycle for waste heat recovery through life-cycle assessment. *Energy*. 56, pp.144 -154.

Murillo, V.B., Rodrigo, S.,Cassiano, M.P., Antonio, C. (2020) Lifecycle assessment of electricity generation. A review of the characteristics of existing literature. International Journal of Lifecycle Assessment. 25(1), pp. 36 - 54

Meyer, L., George, T., Buchgeister, J., Liselotte, S. (2009). Exergoenvironmental analysis for evaluation of the environmental impact of energy conversion systems. *Energy*, 34, pp. 75 -89

Roy, D. and Ghosh, S. (2017). Energy and exergy analysis of an integrated biomass gasification combined cycle employing solid oxide fuel cell and organic Rankine cycle. *Clean Technologies and Environmental Policy*. 19, pp. 1693-1709.

Song, J., Gu, C., Ren, X. (2016). Parametric design and off-design analysis of organic Rankine cycle (ORC) system. *Energy Conversion and Management*. 112, pp. 157-165.

Ssali, M.N., Jiangguo,Du, Duncan, O.H., Mensah, I.A. (2018). Impact of economic growth, energy use and population growth on carbon emission in Sub-Saharan Africa. *Journal of Environmental Science and Engineering*. 7, pp. 178 - 179

Ukemeobong, E.A., Bassey D.N., Agnes E.O., Oyongha, M.A., Remigus, A.U., Obasi-Sam. O., and Patrick, O.O. (2023). Emission based environmental impact analysis from a power-cooling organic Rankine cycle with Ejector system *Scope*, 13(4), pp. 801 - 814

Wang, J. F., and Dia, Y. P. (2009). Energy analysis and parametric optimization for different cogeneration power plant in cement industry. *Applied Energy,* 86(6), pp. 941 - 948.

Yang, M., Li, X., and Wang, L. (2022). Energy and exergy analysis of a cooling/power co-generation Ejector refrigeration System. *Journal of Thermal Science*. 31, pp. 448-462.

Zhang, X., Yu, B., Wang, C. (2014). Comprehensive evaluation index and performance analysis of organic Rankine cycle system considering environmental impact. *Chemical Industry and Engineering Society of China Journal,* 65 (12), pp. 4978-84.

Zhang, S. and Cheng, Y. (2017). Performance improvement of an ejector cooling system with thermal pumping effect (ECSTPE) by doubling evacuation chambers in parallel. *Applied Energies*. 187, pp. 679-688

.